TID-4500, UC-38
Engineering and Equipment

LAWRENCE LIVERMORE LABORATORY
University of California/Livermore, California/94550

UCRL-51250

CALCULATING STRESSES IN A PRESSURE VESSEL WITH FILL TUBE: COMPARISON OF THE FINITE ELEMENT AND PHOTOELASTIC METHODS

R. E. Blum
W. F. Kirkwood

MS. date: June 30, 1972

Contents

CALCULATING STRESSES IN A PRESSURE VESSEL WITH FILL TUBE: COMPARISON OF THE FINITE ELEMENT AND PHOTOELASTIC METHODS

Abstract

We have calculated the stresses in an elastic solid by both the finite element and photoelastic methods. The problem chosen was stress under pressure loading near a pressure-vessel/fill-tube interface, where large stress gradients are present. The two methods gave essentially the same results except in regions of extremely large stress gradients, where the fringes for the photoelastic model were very difficult to separate.

Introduction

The stresses in an elastic solid can be determined by photoelastic or numerical finite element methods. We have compared these methods by using them to calculate the stresses in the pressure vessel shown in Fig. 1.

The calculations were to provide an accurate description of the state of stress existing at design pressure loading, in particular, the large stress gradients near the pressure-vessel/fill-tube interface. Descriptions of the finite element and photoelastic methods are given in Appendix A and Appendix B, respectively.[1]

In the interests of simplicity, the pressure vessel and fill tube are of the same material. They are glued together, and linear elastic behavior is assumed.

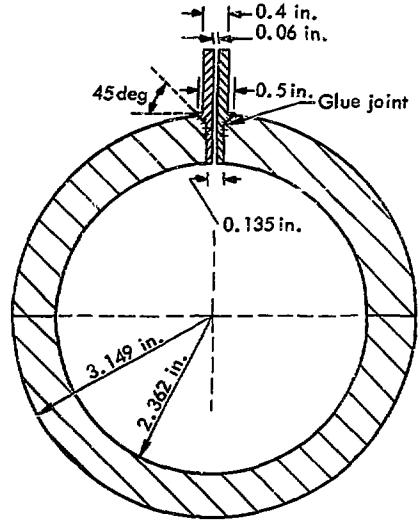

Fig. 1. Model studied: a spherical pressure vessel. The fill tube is glued into place. A 1-mil gap between the fill tube and pressure vessel extends up to the glue joint.

1. An excellent introduction to the finite element method is given in: W. C. Paulsen, Machine Design 43, Sept. 30, Oct. 14, Oct. 28 (1971).

However, in a real pressure vessel the fill tube and pressure vessel are generally of different materials and will be joined by welding or brazing. Also, local yielding may occur at the vessel/tube interface. The presence of different materials and local yielding presents no difficulty for a finite element analysis, and in theory the stresses due to welding can be considered, provided that the effect of the welding process on the properties of the materials is completely defined, which it is not. The photoelastic method cannot account for local yielding or welding stresses. In theory, it can account for different materials, but the difficulty of finding suitable photoelastic materials with correct ratios of material stiffnesses cannot always be overcome.

Finite Element Analysis

We used the NAOS finite element code to determine the stresses in the pressure vessel shown in Fig. 1. The pressure vessel was zoned in two stages. The first finite element zoning is shown in Figs. 2 and 3. Isostress contours of the calculated radial stress (σ_r), axial stress (σ_z), hoop stress (σ_θ), and shear stress (σ_{rz}) are plotted in Figs. 4 through 7. All stresses are nondimensionalized with respect to the internal pressure (i.e., the stress is divided by the internal pressure). Due to the high stress gradients near the tip of the glue joint a finer finite element zoning was made in this region. Figure 8 show this finer zoning. The boundaries of the region shown in Fig. 8 not acted upon by direct pressure were constrained by displacement boundary conditions as calculated by the previous coarser zoning. Isostress contours of σ_r, σ_z, σ_θ, and σ_{rz} are plotted in Figs. 9 through 12.

In a typical finite element stress analysis the calculated stresses are substituted into a failure criterion. For example, contour plots of the von Mises stress are used to predict yielding of a ductile material. The stress pattern calculated at the tip of the glue joint can be used with fracture-mechanics theory to predict local crack growth, i.e., brittle failure due to crack propagation. The failure analysis was not made here since the purpose of this investigation was to compare the calculated stresses with those determined by the photoelastic method.

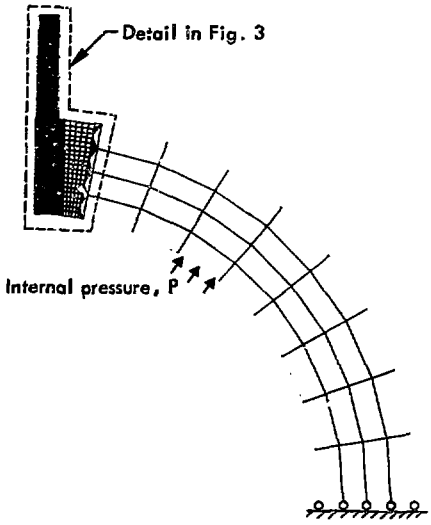

Fig. 2. Zoning for the finite element calculation. The fill-tube/pressure-vessel joint is shown in detail in Fig. 3.

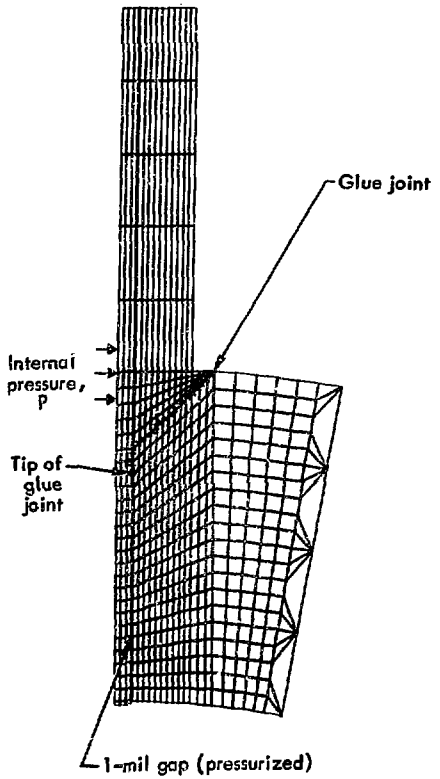

Fig. 3. Zoning at the fill-tube/pressure-vessel joint for the finite element calculation.

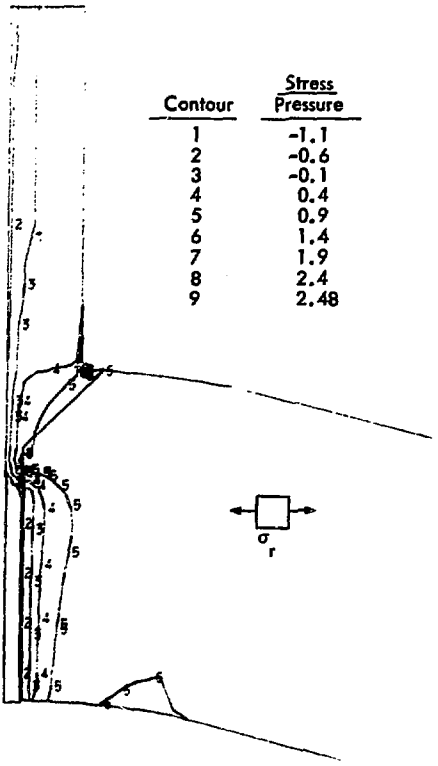

Fig. 4. Isostress contours of the finite-element-calculated radial stress, σ_r.

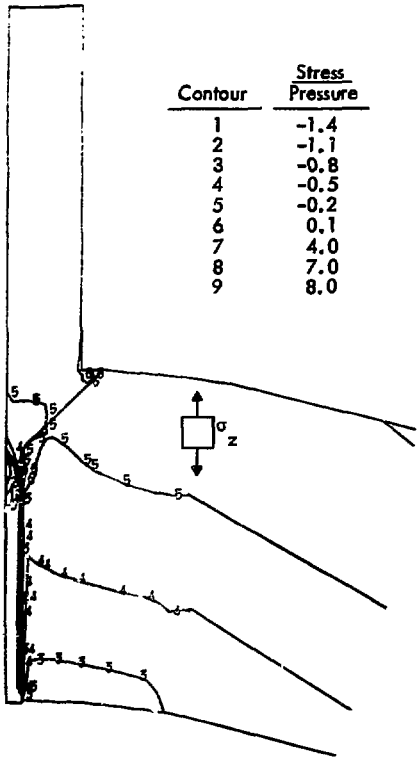

Fig. 5. Isostress contours of the finite-element-calculated axial stress, σ_z.

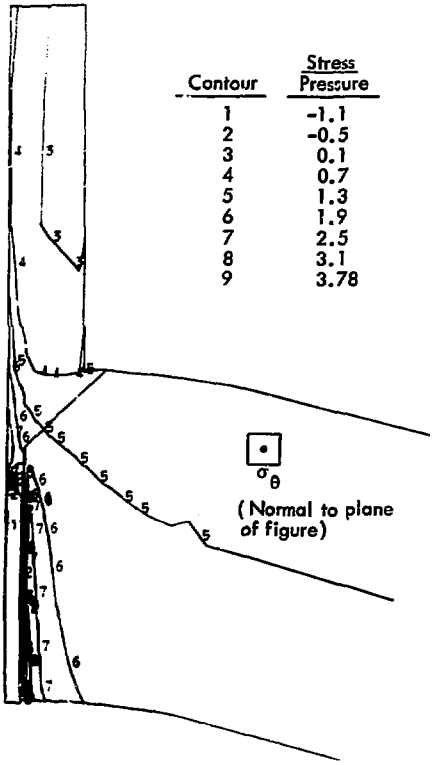

Fig. 6. Isostress contours of the finite-element-calculated hoop stress, σ_θ.

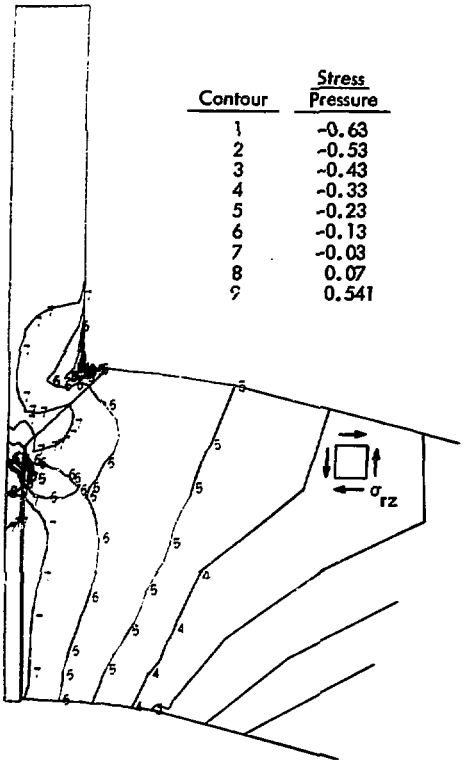

Fig. 7. Isostress contours of the finite-element-calculated shear stress, σ_{rz}.

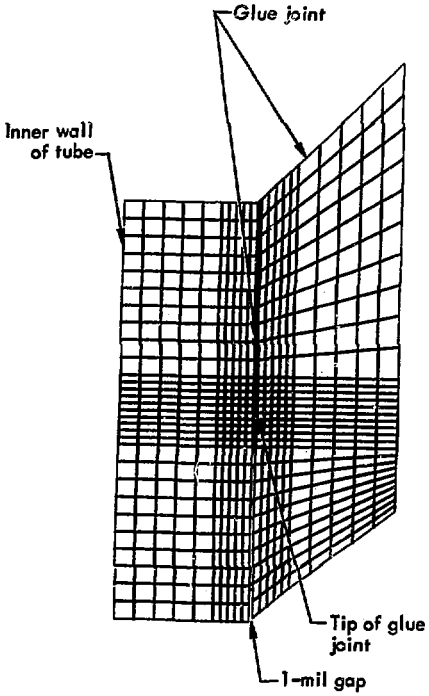

Fig. 8. Finer zoning for the finite element calculation near the tip of the glue joint.

Contour	Stress Pressure
1	-1.2
2	-0.2
3	0.8
4	1.8
5	2.8
6	3.8
7	4.8
8	5.8
9	8.71

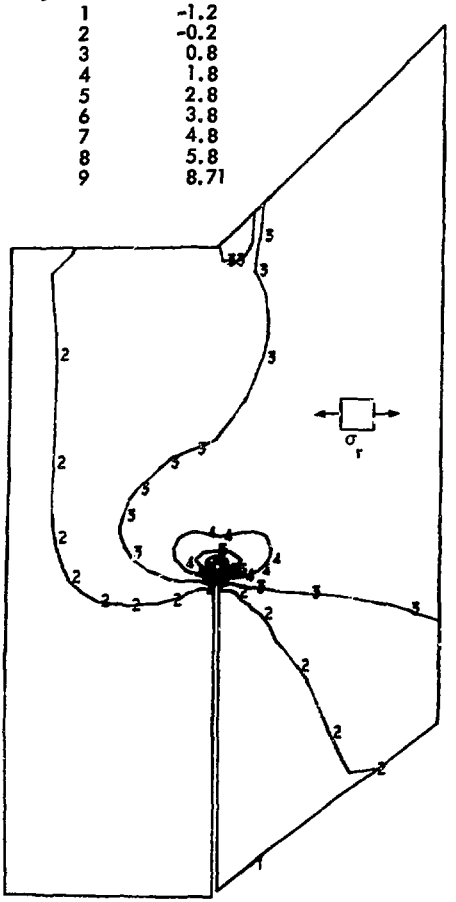

Fig. 9. Isostress contours for the radial stress near the tip of the glue joint (finite element calculation).

Contour	Stress Pressure
1	-1.9
2	-1.2
3	-0.5
4	0.2
5	0.9
6	1.6
7	2.3
8	3.0
9	3.65

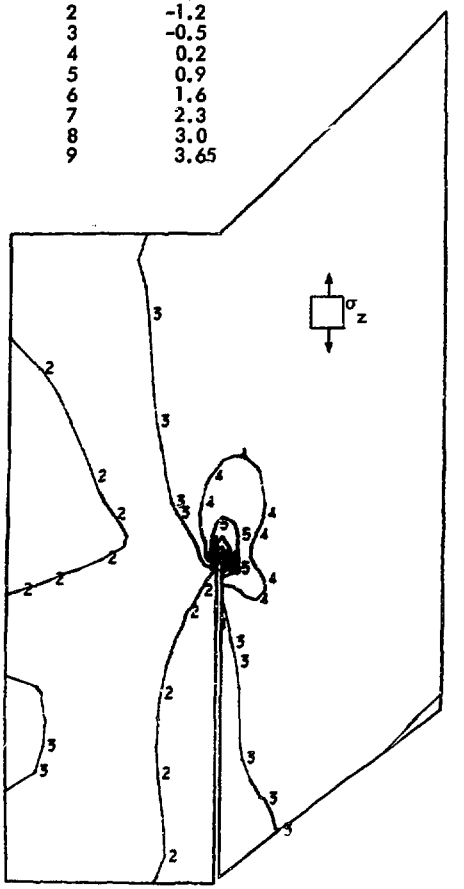

Fig. 10. Isostress contours for the axial stress near the tip of the glue joint (finite element calculation).

Contour	Stress Pressure
1	-1.0
2	-0.2
3	0.6
4	1.4
5	2.2
6	3.0
7	3.8
8	4.6
9	5.3

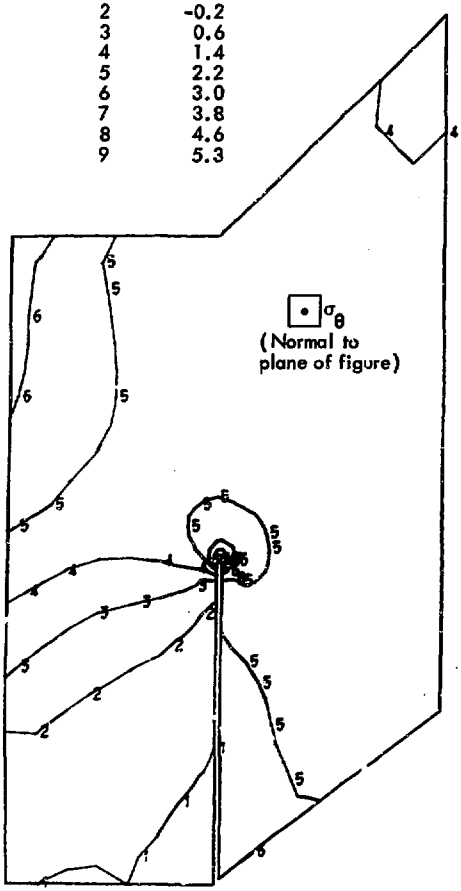

Fig. 11. Isostress contours for the hoop stress near the tip of the glue joint (finite element calculation).

Contour	Stress Pressure
1	-2.3
2	-1.8
3	-1.3
4	-0.8
5	-0.3
6	0.2
7	0.7
8	1.2
9	1.76

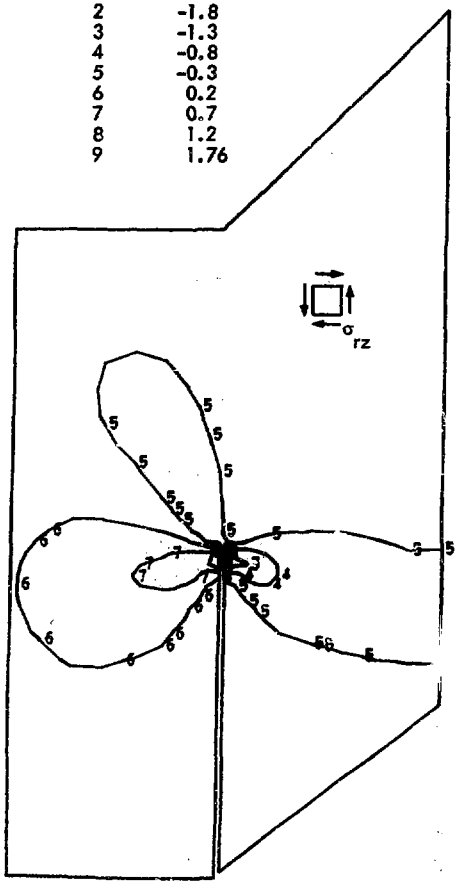

Fig. 12. Isostress contours for the shear stress near the tip of the glue joint (finite element calculation).

Results of the Photoelastic Analysis and Comparison with the Finite Element Solution

A full-scale photoelastic model of the pressure vessel shown in Fig. 1 was fabricated and was tested using stress-freezing and slicing techniques. The model material was a hexahydrophthalic–phthalic anyhydride cured epoxy resin.

The results of the photoelastic analysis and corresponding results for the finite element solution are compared in Figs. 13 through 17.

Figure 13 is a plot of the meridional and radial stresses across the pressure-vessel wall at a section not influenced by

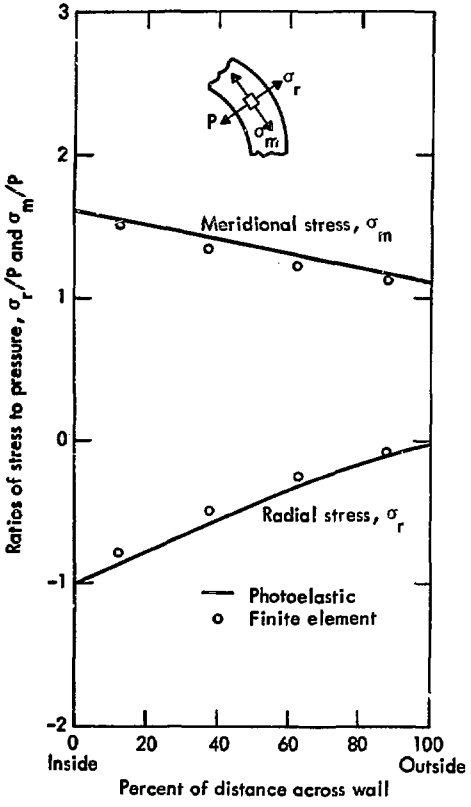

Fig. 13. Comparison of photoelastic and finite element calculations of stresses across the pressure vessel wall.

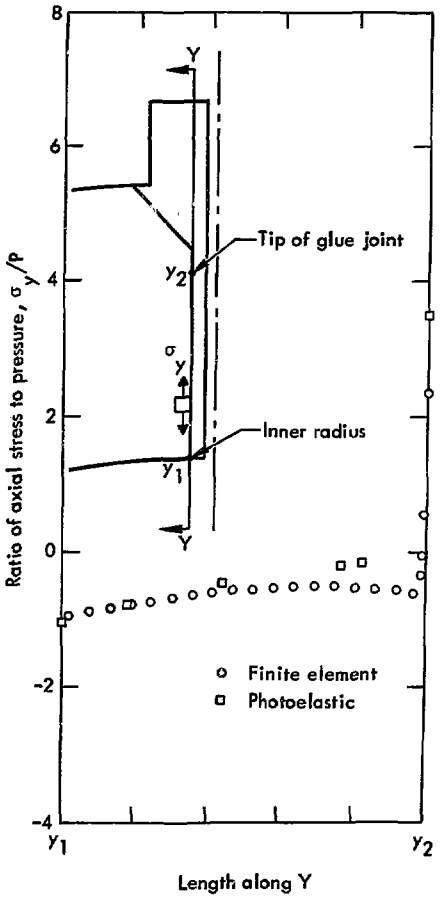

Fig. 14. Finite element and photoelastic calculations of axial stress across section Y-Y.

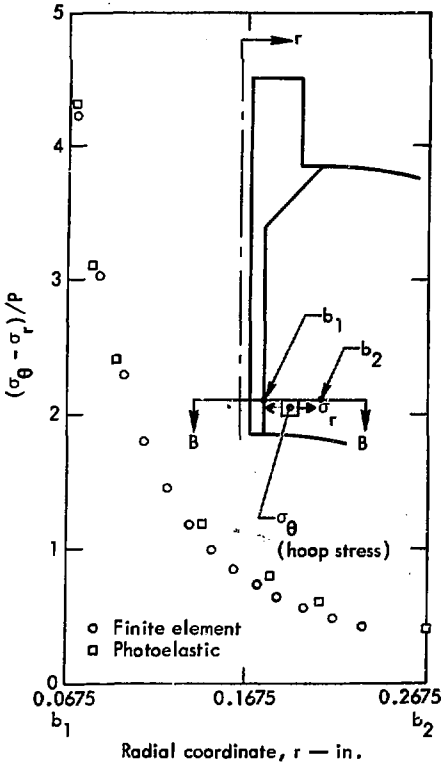

Fig. 15. Finite element and photoelastic calculations of hoop stress minus radial stress across section B-B. Hoop stress is directed perpendicular to the plane of the paper.

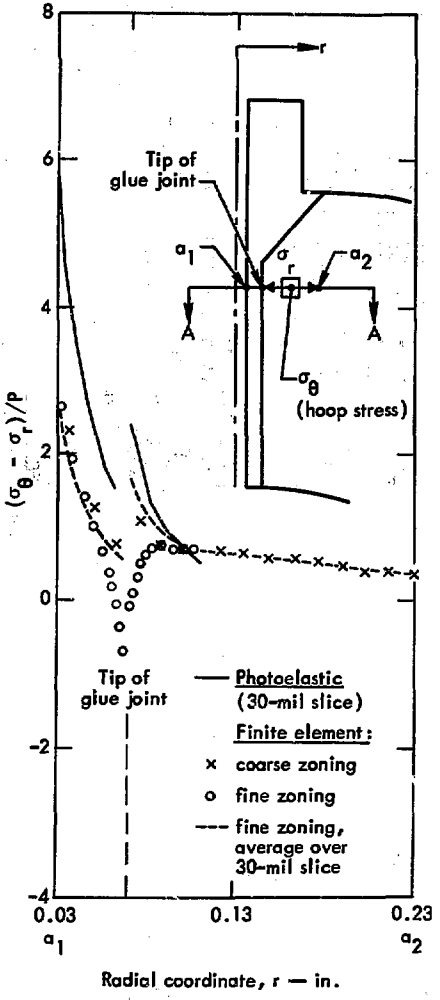

Fig. 16. Finite element and photoelastic calculations of hoop stress minus radial stress across section A-A.

the fill tube. The meridional and radial stress are seen to be in excellent agreement.

Figure 14 is a plot of the axial stress along the interface between the pressure vessel and the fill tube. Again the results show excellent agreement away from the tip of the glue joint. Agreement decreases as the tip of the glue joint is approached. Lack of agreement at the tip of the glue joint is due to the finite element zoning, which did not account for the difference in material properties between the glue and shell, or for the finite radius of the tip of the glue joint (see Fig. 8 for finite element zoning).

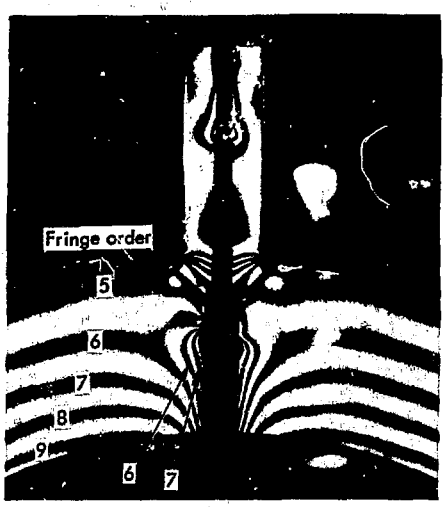

Whole-order fringes taken off the photoelastic model.

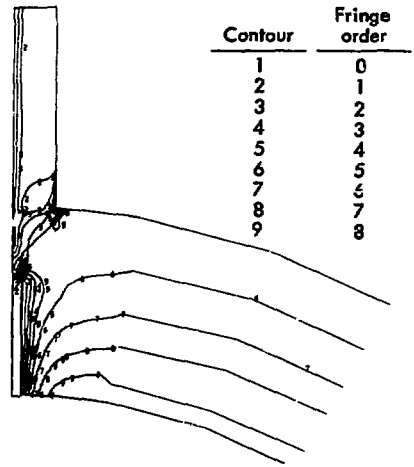

Contour	Fringe order
1	0
2	1
3	2
4	3
5	4
6	5
7	6
8	7
9	8

Whole-order fringes calculated with the finite element method.

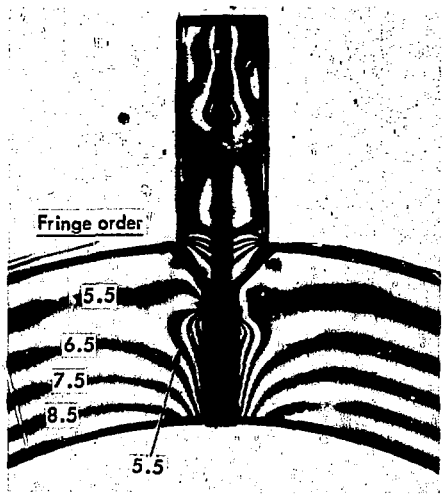

Half-order fringes taken off the photoelastic model.

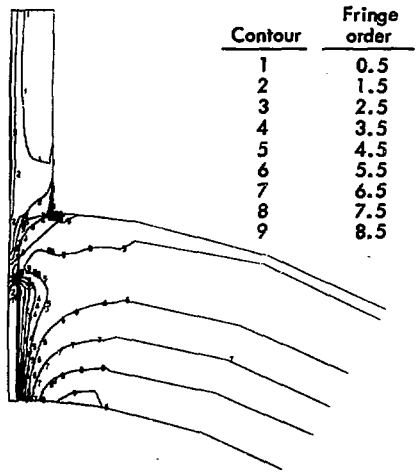

Contour	Fringe order
1	0.5
2	1.5
3	2.5
4	3.5
5	4.5
6	5.5
7	6.5
8	7.5
9	8.5

Half-order fringes calculated with the finite element method.

Fig. 17. Comparison of experimental stress fringe patterns from the photoelastic model with stress fringe plots calculated by the finite element method. Fringes were multiplied by 5 in the polariscope setup.

Figure 15 is a plot of the difference in the hoop and radial stresses in a section perpendicular to the axis of the fill tube near the inner surface of the pressure vessel. (Note that the difference in the hoop and radial stresses is proportional to the fringe orders appearing on the photoelastic slice.) Again, agreement between the two methods of analysis is excellent.

Figure 16 is a plot of the difference in the hoop and radial stresses in a section through the tip of the glue joint and perpendicular to the axis of the fill tube. The correlation in the stresses is at best only fair. The stresses as determined by the photoelastic solution in Fig. 16 average the stresses over a 30-mil slice centered about the tip of the glue joint. The corresponding stresses as determined by the finite element solution average the stresses over a 2-mil thickness, i.e., thickness of one finite element zone (circled points) and a 30-mil thickness (dashed lines). The stresses for the circled data points and dashed line were obtained from the finer zoning shown in Fig. 8. The stresses as determined by the coarser zoning in Fig. 2 are plotted as x's. The x data points average the stresses over a 60-mil thickness. The fact that the finite element solution obtained by the coarse zoning and fine zoning show excellent agreement for the 30-mil and 60-mil thickness averages, plus the excellent agreement with the photoelastic solution seen in Figs. 13 through 15, lead to the conclusion that the stresses plotted in Fig. 16 for the photoelastic solution are incorrect. It should be noted that the photoelastic solution was extremely difficult to obtain in this region due to the large stress gradients, which made fractional fringe counting correspondingly difficult and the position of principal planes hard to orient.

An additional comparison of the results of the photoelastic method and the finite element method is given in Fig. 17. This figure shows photographs of the whole-order and half-order fringes taken off the photoelastic model, and compares them with plots of the whole-order and half-order fringes as calculated by the NAOS code. (The fringe order is proportional to the maximum shear stress.) Correlation is good except in the protruding section of the tube. Lack of correlation in the neck of the tube is due to the coarse zoning in this area in the finite element solution. The slight difference in the fringes in the wall of the pressure vessel (away from the tube) is due to the method in which the plotting routine averaged the stresses at the boundary elements. The correlation in this area is excellent, as was shown in Fig. 13.

Conclusions

The photoelastic method and finite element method were used to calculate the stresses in a pressure vessel with fill tube. As expected, the results of the two methods showed good correlation (except in Fig. 16 as discussed above).

The results of the analysis indicate that either the photoelastic method or the

finite element method can be used to determine the stresses in an elastic solid with essentially the same results. The primary advantage of the finite element method over the photoelastic method is its ability to consider yielding, prestresses, and any number of different materials. The disadvantage of the finite element method is the large computer storage requirement. The computer storage available can seriously limit the number of allowable elements and thereby the resulting accuracy of the solution.

While the general trend in stress analysis is to favor the finite element method over the photoelastic method, the photoelastic method continues to have its place in the solution of complex three-dimensional problems. The photoelastic method is also used to check the results of finite element solutions. The comparison of results between photoelastic and finite element solutions is especially valuable for checking out (debugging) new finite element codes.

Appendix A

Finite Element Method

The finite element method is a numerical technique for obtaining a solution to a partial differential equation. The method has been used extensively in the area of solid mechanics, for which numerous structural dynamic and static finite element computer codes have been developed.

The NAOS code[1] is a finite element program that solves for the stresses in an elastic solid of revolution subjected to symmetric and nonsymmetric static loads. The following is a brief description of the theory behind the NAOS code for the case of symmetric loading and isotropic material properties.

$$\{\sigma\} = \begin{Bmatrix} \sigma_r \\ \sigma_z \\ \sigma_\theta \\ \sigma_{rz} \end{Bmatrix} = \text{stress vector}$$

$$\{\epsilon\} = \begin{Bmatrix} \epsilon_r \\ \epsilon_z \\ \epsilon_\theta \\ \epsilon_{rz} \end{Bmatrix} = \text{strain vector}$$

$$\{p\} = \begin{Bmatrix} p_r \\ p_z \end{Bmatrix} = \text{body force vector}$$

$$\{u\} = \begin{Bmatrix} u_r \\ u_z \end{Bmatrix} = \text{displacement vector}$$

VARIATIONAL FORMULATION OF AXISYMMETRIC ELASTICITY PROBLEM

$$\pi = \int_R \left[\frac{1}{2} \{\sigma\}^T \{\epsilon\} - \{p\}^T \{u\} \right] dv - \int_S \{f\}^T \{u\}\, dS, \qquad (1)$$

where π is the total potential energy in the region R bounded by the surface S (see Fig. A-1).

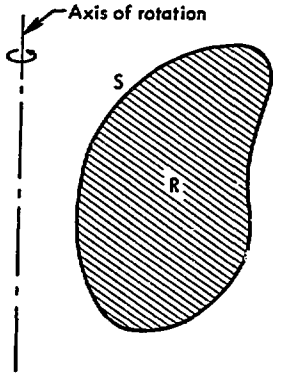

Fig. A-1. Cross section of an axisymmetric region, R, to be treated by the finite element method.

1. R.S. Dunham and R.E. Nickell, Finite Element Analysis of Axisymmetric Solids with Arbitrary Loadings, Structural Engineering Laboratory, University of California, Berkeley, Rept. 67-6 (1967).

$$\{f\} = \begin{Bmatrix} f_r \\ f_z \end{Bmatrix} = \text{surface traction vector}$$

The solution to this elasticity problem is obtained by minimizing the total potential energy, π, subject to imposed displacement boundary conditions, and the following stress-strain and strain-displacement equations.

STRESS-STRAIN EQUATION

$$\{\sigma\} = [D]^{-1}\{\epsilon\}, \qquad (2)$$

where

$$[D] = \frac{1}{E}\begin{bmatrix} 1 & -\nu & -\nu & 0 \\ -\nu & 1 & -\nu & 0 \\ -\nu & -\nu & 1 & 0 \\ 0 & 0 & 0 & 2(1+\nu) \end{bmatrix}$$

E = Young's modulus

ν = Poisson's ratio.

STRAIN-DISPLACEMENT EQUATION

$$\{\epsilon\} = [B]\{u\}, \qquad (3)$$

where

$$[B] = \begin{bmatrix} \frac{\partial}{\partial r} & 0 \\ 0 & \frac{\partial}{\partial z} \\ \frac{1}{r} & 0 \\ \frac{\partial}{\partial z} & \frac{\partial}{\partial r} \end{bmatrix}$$

r = radial coordinate

z = axial coordinate.

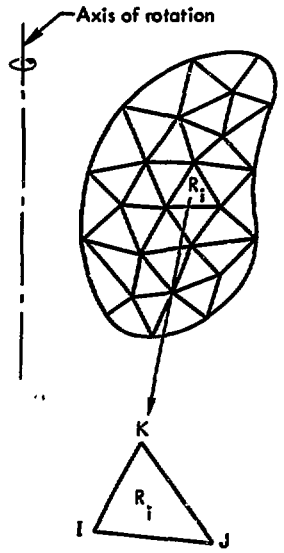

Fig. A-2. Subdivision of the region R into triangular subregions, one of which is R_i.

Substituting Eqs. (2) and (3) into Eq. (1) yields

$$\pi = \int_R \left[\frac{1}{2}\{u\}^T[B]^T[D]^{-1}[B]\{u\} - \{p\}^T\{u\}\right] dV - \int_S \{f\}^T\{u\}\, dS. \qquad (4)$$

In the finite element method, the above integral is approximated by dividing R in subregions R_i, and specifying shape functions for the dependent variables, $\{u\}$, over each subregion. In the NAOS code, the subregions are circular rings with triangular cross sections as shown in Fig. A-2. (Note that quadrilateral cross-section elements are also allowable in NAOS. The code automatically subdivides

quadrilaterals into four triangular cross-section elements.) Over the subregion R_i the following shape function is assumed

$$\{u_i\} = [N_i]\{\alpha\}, \tag{5}$$

where

$$[N_i] = \begin{bmatrix} 1 & r & z & 0 & 0 & 0 \\ 0 & 0 & 0 & 1 & r & z \end{bmatrix}$$

$$\{\alpha\} = \begin{Bmatrix} \alpha_1 \\ \alpha_2 \\ \alpha_3 \\ \alpha_4 \\ \alpha_5 \\ \alpha_6 \end{Bmatrix}.$$

Writing Eq. (5) at points I, J, and K yields

$$\begin{Bmatrix} \{u_i\}_I \\ \{u_i\}_J \\ \{u_i\}_K \end{Bmatrix} = \begin{bmatrix} [N_i]_I \\ [N_i]_J \\ [N_i]_K \end{bmatrix} \{\alpha\}.$$

Solving for $\{\alpha\}$ and substituting into Eq. (5) yields

$$\{u_i\} = [N_i] \begin{bmatrix} [N_i]_I \\ [N_i]_J \\ [N_i]_K \end{bmatrix} \begin{Bmatrix} \{u_i\}_I \\ \{u_i\}_J \\ \{u_i\}_K \end{Bmatrix} = [\bar{N}_i]\{\bar{u}_i\}. \tag{6}$$

Substituting the above expression for $\{u_i\}$ into Eq. (4) yields

$$\pi = \sum_i \left[\int_{R_i} \frac{1}{2} \left[\{\bar{u}_i\}^T [\bar{N}_i]^T [B]^T [D]^{-1} [B] \cdot [\bar{N}_i]\{\bar{u}_i\} - \{p\}^T [\bar{N}_i]\{\bar{u}_i\} \right] dR_i - \int_{S_i} \{f\}^T [\bar{N}_i]\{\bar{u}_i\}\, dS_i \right].$$

The indicated integrations are now carried out either analytically or numerically to yield

$$\pi = \sum_i \left[\frac{1}{2} \{\bar{u}_i\}^T [K_i]\{\bar{u}_i\} - \{P_i\}^T\{\bar{u}_i\} - \{F_i\}^T\{\bar{u}_i\} \right], \tag{7}$$

where

$$[K_i] = \int_{R_i} [\bar{N}_i]^T [B]^T [D]^{-1} [B] [\bar{N}_i]\, dR_i$$

$$\{P_i\}^T = \int_{R_i} \{p\}^T [\bar{N}_i]\, dR_i$$

$$\{F_i\}^T = \int_{S_i} \{f\}^T [\bar{N}_i]\, dS_i.$$

Note that the integral over S_i only applies to a subregion R_i with one or more sides on the boundary of R.

Now, define a vector $\{U\}$ for the displacements at all the node points in R, i.e., the displacements of the corners of all the triangular subregions (elements) R_i.

$$\{U\} = \begin{Bmatrix} \{u_1\} \\ \{u_2\} \\ \{u_3\} \\ \vdots \end{Bmatrix}.$$

In terms of $\{U\}$ Eq. (6) can be written as

$$\pi = \sum_i \left[\frac{1}{2} \{U\}^T [\bar{K}_i] \{U\} - \{\bar{P}_i\}^T \{U\} - \{\bar{F}_i\}^T \{U\} \right]$$

or

$$\pi = \frac{1}{2} \{U\}^T [K] \{U\} - \{P\}^T \{U\} - \{F\}^T \{U\}.$$

Minimizing with respect to $\{U\}$ yields

$$[K]\{U\} - \{P\} - \{F\} = 0. \qquad (8)$$

Equation (8) is solved subject to any displacement boundary conditions to yield the displacement $\{U\}$ in the region R. The strains in a subregion R_i are determined by using Eqs. (3) and (6), i.e.,

$$\{\epsilon_i\} = [B][\bar{N}_i]\{\bar{u}_i\},$$

and the stresses by Eq. (2), i.e.,

$$\{\sigma_i\} = [D]^{-1}\{\epsilon_i\}.$$

Appendix B
Photoelastic Method

The photoelastic method for solving the state of stress in both two- and three-dimensional structures problems is widely employed in industry. Typical problems solved by this technique are:

- Stresses in solid-propellent motors—Aerojet General Corporation.
- Stresses in tube sheets and pressure-vessel reactors—Westinghouse Research Corporation.
- Determination of stresses in reinforced openings in pressure vessels. Nearly 100 vessels were tested by the University of Illinois and Westinghouse Research Corporation for the Pressure Vessel Research Committee of the Welding Research Council.[2]
- Oak Ridge National Laboratory—nuclear pressure-vessel reactors.

In other words, the photoelastic technique is a useful tool that is used in designing nuclear-reactor pressure vessels, the related tube sheets to these designs, and any other nonsymmetrical shell designs not covered by existing finite element stress-analysis codes. The staff of Combustion Engineering, Inc., at Windsor, Connecticut, has been combining the results of the photoelastic methods and the finite element codes for basing design criteria for pressurized shells. Other structural problems solved by this technique are bridges, tunnels, engine components, etc.

FUNDAMENTAL PRINCIPLES AND STRESS OPTIC EQUATIONS

The photoelastic models used by most investigators are clear plastics in flat sheet form for two-dimensional stress analysis. For three-dimensional analysis, carefully selected Epoxy and hardener combinations are used.

When a transparent material is viewed in plane polarized light and a load is applied across some boundary, a series of colored bands will appear that represent a locus of all points along which the difference in the principal stresses (P - Q) are equal. If a proper filter is placed in the path of light such that the light has a constant wave length λ, the colored bands will appear as alternate black and white bands which are more convenient for photography and stress analysis purposes. These bands appear in a numbered order easily identified in white light because the zero order fringe is black. The following nomenclature lists the fundamental terminology employed in photoelastic stress analysis:

λ = wavelength (in. or Å)

c = stress optical coefficient ($in.^2/lb$)

t = model thickness (in.)

P, Q = the two principal stresses ($lb/in.^2$)

n = number of fringes, or fringe order

2. Welding Research Council Bulletin 113, April 1966.

$f = \lambda/c$ = material fringe value (lb/in.-fringe)

τ = shear stress

σ_m, σ_r = principal stresses in example 2

The Stress-Optic law expressed in terms of fringe order may be written as:

$$n\lambda = t(P - Q) \tag{9}$$

and

$$(P - Q) = \frac{n\lambda}{ct}.$$

Let the constant terms $\frac{\lambda}{c} = f$, and the final equation universally employed in photoelastic stress analysis becomes

$$(P - Q) = \frac{nf}{t}. \tag{10}$$

Fringe orders viewed in a polariscope or a photograph using monochromatic light are counted as whole numbers in a dark field or half orders in light field. These fields are changed from dark to light by rotating one of the elements (quarter-wave plate) of the polariscope. For illustrative purposes in reports, it is usually more convenient to use the light-field photograph for marking in fringe orders on the light background.

EXAMPLE PROBLEM 1

Figure B-1 is an example of applying the fundamental principles of photoelastic stress analysis. This plane-stress solution to a simple problem shows excellent correlation to the theoretical result using the flexure equation.

THREE-DIMENSIONAL PHOTOELASTIC STRESS ANALYSIS

Three-dimensional problems in photoelasticity are handled by one of three methods: the frozen-stress technique, the scattered-light technique, and the buried-polariscope technique. The results in this report were obtained by the frozen-stress technique, which is the most popular and easily handled.

Models of structures to be evaluated may often be reproduced in full or reduced scale epoxy models (shells, rings, forgings, beams, etc.). The models may then be loaded at the same boundary points and by applying the principles of dimensional analysis, the model stresses may be related to prototype stresses. For axisymmetric pressurized shells of revolution the elastic analysis is simplified by the fact that model-prototype stresses are directly related by geometry ratios. For example, the maximum stress in a thick-walled sphere, internally pressurized, is:

$$\sigma = p\frac{(b^3 + 2a^3)}{2(b^3 - a^3)}, \tag{11}$$

where

p = internal pressure in psi

a = inside radius in inches

b = outside radius in inches

Now if both sides of the above equation are divided by "p", then it is readily seen that the σ/p ratio for a model is the same as that of the prototype with similar radius

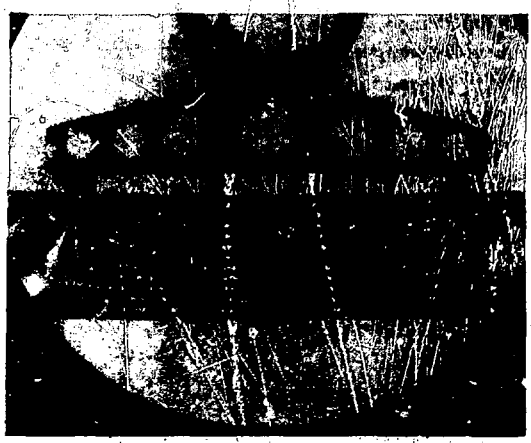

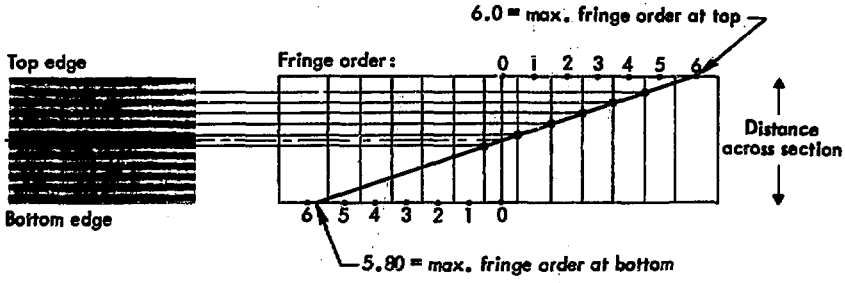

Fig. B-1. An example of applying the fundamental principles of photoelastic stress analysis. Part (a) shows the light-field photograph of half-order stress fringes of a beam in pure bending (m = 86.8 in.-lb, f = 88 lb/in.-fringe, the beam is 1 in. deep by 0.250 in. thick, the average fringe at the outer fiber is 5.90, the material is allyl diglycol carbonate). Part (b) shows how the fringe-order data taken from the photograph is plotted and extrapolated to the edges of the beam to determine the maximum fringe order. From this value of n the maximum principal stress can be determined (σ_{max} = nf/t, = (5.9 × 88)/0.250 = 2070 psi). The theoretical maximum principal stress, $\sigma_{theor.}$ is calculated as mc/I, or (86.8 × 0.5 × 12)/(0.250 × 1) = 2080 psi.

ratios. Then to calculate prototype stresses, use the equation:

$$(\sigma/p)_m = (\sigma/p)_p, \qquad (12)$$

where the subscripts refer to the model and prototype, respectively.

Stress freezing is accomplished by placing the model in an oven and while under load, heating the model to the critical temperature of the epoxy. For most tests at LLL, we use an epoxy with a critical temperature of approximately 315°F. At this temperature the modulus reduces to about 5000 psi and the material

fringe value $f \cong 1.70$ lb/in. fringe. The model deforms, and when the temperature is reduced to ambient with the load still applied, all the deformations and stresses remain "locked in." Subsequent slices removed and polished may be treated in most cases as a plane-stress problem if the model is axisymmetric and sliced along a principal plane.

EXAMPLE PROBLEM 2

Figure B-2 shows a thick-walled pressurized shell that has been sliced on a great circle plane of symmetry passing through the tube at the pole. Earlier in this report we compared the photoelastic and finite element solutions for this model. Stresses along the vertical wall of the hole in the shell were analyzed from this slice. Hoop stresses in the hole were also evaluated from further subslices of this part.

In most three-dimensional problems, boundary stresses are of primary interest, because most failures occur at boundaries. For our model the boundary stresses may be expressed for the outside:

$$\frac{\sigma_m - \sigma_r}{p} = \frac{nf}{pt}, \quad (\sigma_r = 0)$$

$$\frac{\sigma_m}{p} = \frac{nf}{pt} \tag{13}$$

and for the inside boundary:

$$\frac{\sigma_m - \sigma_r}{p} = \frac{nf}{pt}, \quad (\sigma_r = -p).$$

Therefore:

$$\frac{\sigma_m}{p} = \frac{nf}{pt} - 1. \tag{14}$$

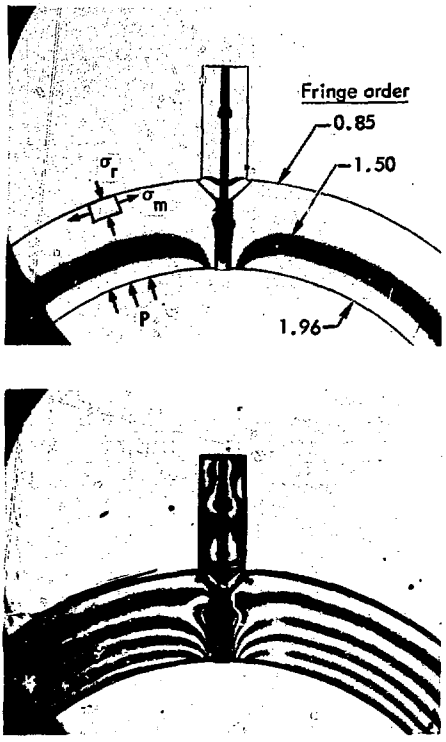

Fig. B-2. Example of determining stresses by photoelastic method. A thick-walled pressure vessel has been sliced on a great-circle plane of symmetry passing through the tube at the pole. Stresses along the vertical wall of the hole in the shell were analyzed from this slice. These are light-field photographs; the lower photograph has the fringes multiplied five times for easier determination of the fractional fringe orders across the field. The model thickness is 0.132 in., and the f is 2.71 lb/in.-fringe.

Hoop stresses along the vertical axis of the hole through the shell were determined from the inner boundary to the end of the tube braze. Equation 14 was used with σ_θ = hoop stress.

Solutions across the field of the slice were performed using the equations of equilibrium in polar form, the principal stresses:

$$\sigma_r = (\sigma_r)_0 + \int \frac{\sigma_m - \sigma_r}{r}\, dr \qquad (15)$$

As $\sigma_r - \sigma_m = \frac{nf}{t}$, (refer to Eq. (10))

$$\sigma_r = p + \int \frac{nf}{t}\,\frac{dr}{r} \qquad (16)$$

Equations 15 and 16 are usually only of academic interest because they provide solutions for the interior stresses, which are primarily lower. Articles on photomechanics frequently appear in the technical journals such as Experimental Mechanics and the Applied Mechanics Journal of ASME. There is an excellent text, "Experimental Stress Analysis" by J. Dally and W. Riley[3] with a section on photoelasticity that is easily read.

---

3. J. W. Dally and W. F. Riley, Experimental Stress Analysis (McGraw-Hill, New York, 1965).

Printed in USA. Available from the National Technical Information Center, National Bureau of Standards, U. S. Department of Commerce, Springfield, Virginia 22151
Price: Printed Copy $3.00; Microfiche $0.65.